Rev. Adv. Mater. Sci. 41 (2015) 84-92

NON-MONOTONOUS MECHANICAL BEHAVIOR AT THE NANOSCALE: STRENGTHENING/SOFTENING OF FLOW CURVES AND NANODEFECT KINETICS

X. Zhang[1], A.E. Romanov[2] and E.C. Aifantis[1,2,3]

[1]School of Mechanics and Engineering, Southwest Jiaotong University,
Key Laboratory of Advanced Technologies of Materials, Ministry of Education of China,
Chengdu 610031, P. R. China
[2]International Laboratory Advanced Nanomaterials and Optoelectronics, ITMO University, Lomonosova 9,
St. Petersburg, 199034, Russia
[3]Lab of Mechanics and Materials, Aristotle University, Thessaloniki 54124, Hellas/Greece

Received: April 19, 2015

Abstract. It is well known that the flow or stress-strain curves of conventional polycrystals level up exhibiting a “hardening” behavior when the grain size is decreasing within the micrometer range. However, when the grain size enters in the 10-20 nm range, an inverse “softening” behavior is observed and the stress-strain curves may become softer than their micrometer counterparts. This behavior is analogous to the Hall-Petch (HP) and inverse Hall-Petch (IHP) observed for the yield strength, as well as for the activation volume and pressure sensitivity parameters discussed in a preceding article. Here we develop a physically-based constitutive model for interpreting the aforementioned size-dependent behavior of the flow curves, in comparison with experimental results for nanopolycrystalline and nanotwins materials. Despite of its simplicity, this is the first physically-based phenomenological model that can describe HP and IHP behavior for flow curves at the nanoscale. A deeper approach for capturing such behavior may rest on structural defect considerations; in particular, the evolution and interaction of the pertinent defect population (dislocations, disclinations, twins) that emerge at the nanoscale. A preliminary discussion of this approach, will also be given herein.

1. INTRODUCTION

In a preceding article (X. Zhang and E.C. Aifantis, Non-monotonous mechanical behavior at the nanoscale: Elastic and plastic properties, *Strength of Materials*, in press) we have employed a simple “rule of mixtures” argument for the “grain interior” and the “grain boundary” spaces or phases, to interpret the non-monotonous behavior of plastic flow parameters (such as yield strength, activation volume, and pressure sensitivity) above and below a characteristic nanoscale grain size. When the “rule of mixtures” argument is extended to include the interaction of the two superimposed phases within a continuum “theory of mixtures” framework, it turns out that the local constitutive equation is generalized to include higher-order gradients of the local strain. The solution of a simple boundary value problem for a typical unit cell material element leads then to a size-dependent expression for the overall “effective” elastic modulus, in agreement with experimental observations. The same can be done for the plastic or hardening modulus. A slight modification of the aforementioned gradient argument for the local response, is employed here to express the above gradient dependence through a microstructural material length such as grain size (d, for nanopolycrystals) or twin lamella thickness (λ, for

Corresponding author: E.C. Aifantis, e-mail: mom@mom.gen.auth.gr

nanotwins). This leads to a modification of the usual macroscopic constitutive equations used for the stress-strain curves of conventional metals by properly bringing into these relationships the parameters d or λ.

A particular stress-strain relationship which has been used with success to fit stress-strain curves for conventional materials with characteristic size at the micrometer level, is the Voce equation [1]. Its modification to include a grain size dependence has been briefly discussed earlier (see, for example, [2,3]), along with its implications to model the corresponding size-dependent flow curves of nanopolycrystals with varying grain size.

In Section 3, we revisit this problem for nanopolycrystals by considering in more detail the HP-IHP behavior of nanocrystalline copper (nc-Cu) specimens with varying average grain size. Size-dependent strain rate and temperature effects are also interpreted through a grain size-dependent Voce model and the same is done for modeling the simultaneous grain size and strain rate dependence of nanocrystalline nickel (nc-Ni) specimens.

Roughly speaking, the gradient plasticity argument used for the above considerations in Section 2 for nanograins, as well in Section 3 for nanotwins, is as follows: strain hardening (or softening) occurs when internal surfaces, such as grain or twin boundaries, act as obstacles (or facilitators) to the motion of dislocations, i.e. the carriers of plastic deformation. The local flow stress, i.e. the local resistance to dislocation motion, would involve a homogeneous part (e.g. a friction stress due to the lattice-dislocation interaction or a homogenized back stress due to the dislocation-dislocation interaction), as well as an inhomogeneous or gradient part (e.g. the local stress concentrators at grain boundaries, grain boundary triple junctions, or grain-twin boundary intersections). Then, at a first approximation, the local expression for the flow stress may be written as $\tau = \tau_0 + kl^{1/2}|\nabla\varepsilon|^{1/2}$ where τ_0 denotes the homogenous part of the flow stress, ε is the strain, k is a strength coefficient and l is an internal length depending, for example, on the dislocation source distance [4]. On applying the above relation to the case of a representative grain boundary or twin lamella unit cell; we can conclude without difficulty that the gradient (i.e. the $|\nabla\varepsilon|^{1/2}$) dependence of the various stress quantities characterizing plastic flow, such as the yield stress and the hardening modulus may be replaced by $d^{-1/2}$ or $\lambda^{-1/2}$ where the parameters (d, λ) denote grain size or twin thickness, respectively. To see this, one may note (on the basis of a scale invariance dimensionless argument) that at the scale level of a nanograin or nanotwin, $\nabla\varepsilon$ may be approximated by ε_0/d or ε_0/λ where ε_0 is a reference strain. Then, by redefining k as $kl^{1/2}\varepsilon_0^{1/2}$, the aforementioned $|\nabla\varepsilon|^{1/2}$ dependence for the yield stress and strain hardening modulus is replaced by a corresponding $d^{-1/2}$ or $l^{-1/2}$ dependence.

2. PHENOMENOLOGICAL STRENGTHENING/SOFTENING MODEL FOR NANOGRAINED METALS

In a previous article [2], a “rule of mixtures” argument was used to model the full size-dependent stress-strain graphs (not just the yield stress) of nanograined metals with varying grain size. This was based on a Voce’s type constitutive relation for the flow stress which was also assumed to obey a modified HP type relation deduced from an argument based on gradient plasticity with interfacial energy [5,6]. An alternative, phenomenologically simpler and robust procedure was adopted later in [3] based on the Voce-type relationship

$$\sigma = \sigma_y + \left(\sigma_s - \sigma_y\right)\tanh\left[\frac{h\varepsilon^p}{\sigma_s - \sigma_y}\right], \qquad (1)$$

where the flow stress-like quantities (σ_y,σ_s,h) designating respectively (friction or initial yield stress, saturation stress, strain hardening modulus) are size-dependent obeying the following HP and IHP relations

$$\sigma_{y,s} = \sigma_{y,s}^0 + k_{y,s}d^{-1/2}, \qquad (2)$$

$$h = h_0 - k_h d^{-1/2}, \qquad (3)$$

where d denotes the grain size, ($\sigma_{y,s}^0$,h_0) and ($k_{y,s}$,k_h) are constants. These equations have been used in [3] to obtain the grain size dependence of the flow curves as shown in Fig. 1a, in comparison with available experimental results [7]. These experimental results show a HP type of “hardening” behavior, i.e. “harder” flow curves with decreasing grain size. On the other hand, “softer” stress-strain curves with decreasing grain size have been obtained through molecular dynamics (MD) simulations [8]. This IHP type of softer behavior for the flow curves is also predicted through the modified grain size-dependent model by using Eqs. (1)-(3), with the following values for the phenomenological coefficients, σ_y^0 = 0.5 GPa, σ_s^0 = 4 GPa, k_s = -140 kPa $m^{1/2}$, h_0 = 730 GPa, and k_h = 34 MPa $m^{1/2}$. This comparison between MD simulations and model predictions are

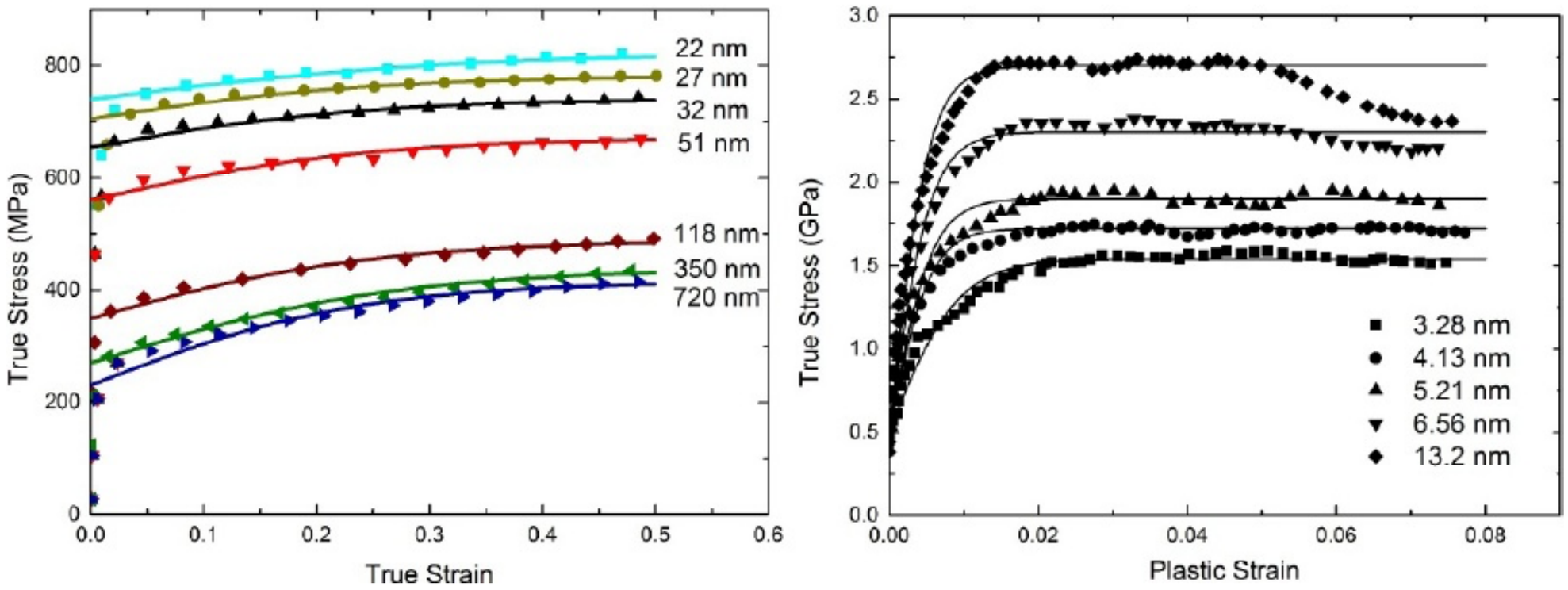

Fig. 1. (a) Fitting the grain size dependence of nanocrystalline copper (nc-Cu) specimens showing a HP type of "hardening" behavior. (b) Comparison between model predictions and simulations for nc-Cu sample of showing a IHP type of "hardening" behavior.

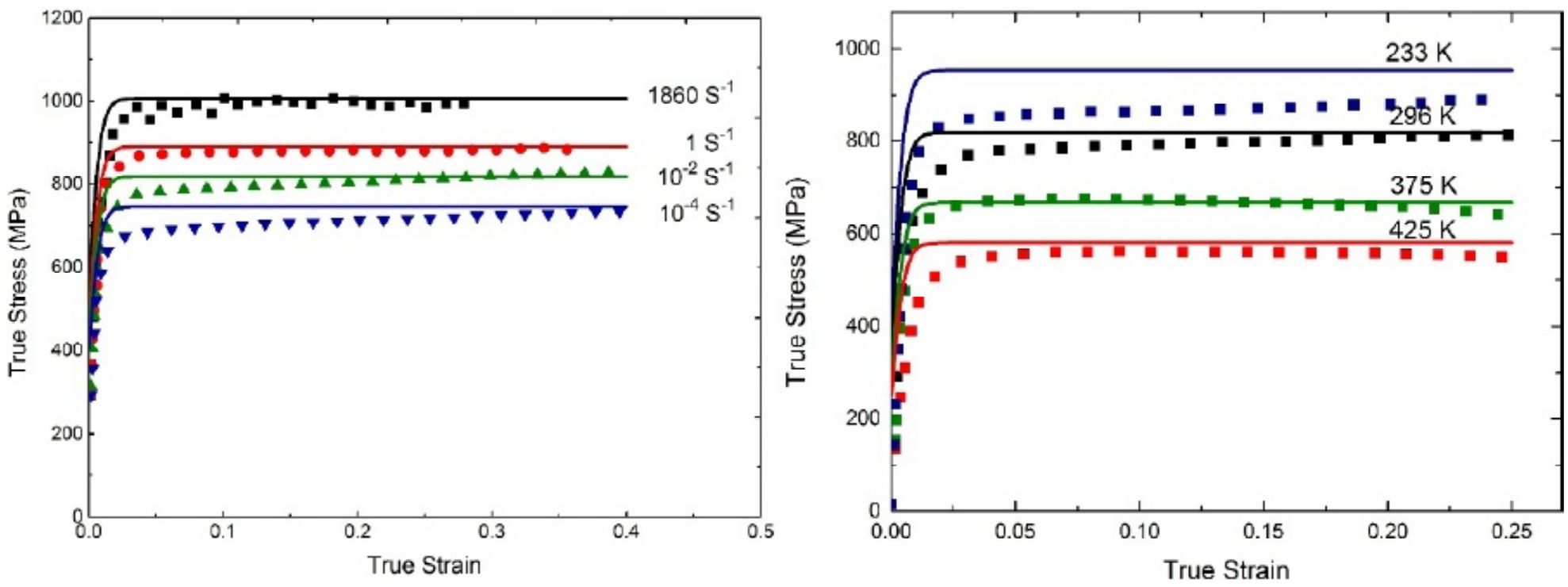

Fig. 2. (a) Fitting the strain rate dependence of nanocrystalline copper (nc-Cu) specimens. (b) Fitting the temperature dependence of nanocrystalline copper (nc-Cu) specimens.

provided in Fig. 1b. These results have also been briefly discussed in [3], but we though to also list them here in more detail, in the context of the present article.

When the interplay between grain size, strain rate and temperature needs to be investigated, Eq. (1) was modified by a multiplicative term of the form $\{1 + c\ln(\dot{\varepsilon}/\dot{\varepsilon}_0)\}$ to include the effect of strain rate $\dot{\varepsilon}$ ($\dot{\varepsilon}_0$ is a reference strain rate and c is a constant), and a term of the form $\{1-[(T-T_g)/(T_m-T_g)]^m\}$ to include the effect of temperature T (T_m is the melting temperature, T_g is a reference temperature and m a constant) in the overall expression for the flow stress. A good comparison between experimental data and model description for ng-Cu was already reported in [3], along with the corresponding choice of the various parameter values for establishing these fits shown in Fig. 2.

The simultaneous effect of both grain size (d) and strain rate ($\dot{\varepsilon}$) dependence on the respective stress-strain curves (i.e. the interplay of d and $\dot{\varepsilon}$ on the mechanical response) for nanocrystalline nickel (nc-Ni) is discussed below. A slightly different form of Voce model (nevertheless equivalent to Eq. (1)) is adopted for this purpose. It reads

$$\sigma = \sigma_s - \left(\sigma_s - \sigma_y\right)\exp\left(-\frac{\Theta_0 \varepsilon^p}{\sigma_s - \sigma_y}\right), \tag{4}$$

where $(\sigma_s,\sigma_y,\varepsilon^p)$ are as before, and Θ_0 denotes the initial strain hardening rate. Motivated by the modified HP/IHP-type expressions deduced in [3] on the basis of a strain gradient theory argument, we assume the following relations for $(\sigma_s,\sigma_y,\Theta_0)$:

$$\begin{aligned}
\sigma_y &= \left(\sigma_{yr} + \frac{k_1}{\sqrt{d}} - \frac{k_2}{d}\right)\left(1 + m_f \ln\left(\frac{\dot{\varepsilon}_p}{\dot{\varepsilon}_p^0}\right)\right), \\
\sigma_s &= \left(\sigma_{sr} + \frac{k_3}{\sqrt{d}} - \frac{k_4}{d}\right)\left(1 + m_s \ln\left(\frac{\dot{\varepsilon}_p}{\dot{\varepsilon}_p^0}\right)\right), \\
\Theta_0 &= \Theta_{0r} + \frac{k_5}{\sqrt{d}} - \frac{k_6}{d}.
\end{aligned} \tag{5}$$

Table 1. Parameter values used for fitting the simultaneous effect of grain size and strain rate on the mechanical response of nc-Ni.

σ_y MPa	σ_{sr} MPa	Θ_{0r} GPa	k_1 MPa nm$^{1/2}$	k_3	k_5	k_2 MPa nm	k_4	k_6	m_f	m_s
78	293	-32	9350	13056	3.83	37366	34536	1.64	0.059	0.017

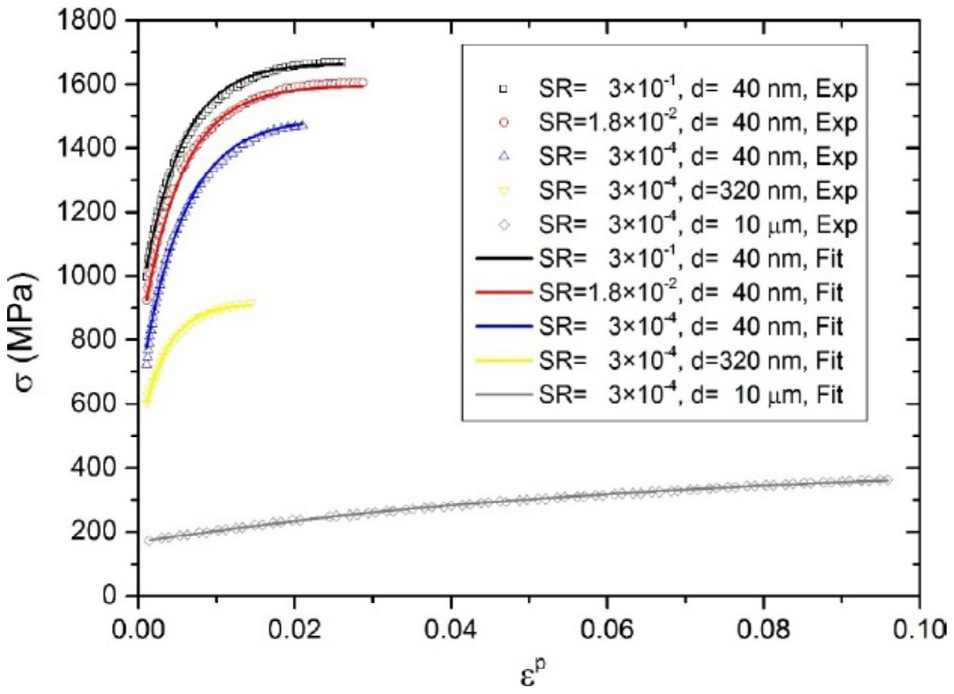

Fig. 3. Fitting the simultaneous effect of grain size and strain rate dependence on the stress-strain response of nc-Ni.

Upon insertion of Eq. (5) into Eq. (4), we obtain an excellent "fit" of the experimental data reported in [9] for nc-Ni specimens with varying grain size under different strain rates, by choosing the model parameters as shown in Table 1.

This fit, which simultaneously captures both the grain size dependence and the strain rate dependence, is shown in Fig. 3. All fitting parameters have physically reasonable values, as compared to those existing in the literature, with the exception of the parameter Θ_0 for which no contact can be established with previous models. It should be pointed out, in this connection, that the choice of the values for the parameters k's and Θ_{0r} is very sensitive to the fitting, while this is not the case for the values of σ_{yr}, σ_{sr}, m_f, and m_s. This provides definite support to the phenomenological model as the range of the values for these last four quantities is known from other independent experiments. It follows that for the parameters k's and Θ_{0r} further laboratory tests, as well as simulations, employing a wide range of grain sizes may be necessary for establishing their physical relevance and meaning.

In view of the above interesting fitting results for nano-grained metals, we show in the next section how one can model in a similar way the unusual stress-strain response of nano-twinned metals (in particular nt-Cu with average grain size of 500 nm). This is simply done by essentially replacing, in the above stated flow stress expression, the dependence on the grain size (d) with the twin lamella thickness (λ). Cooperative effects between grain boundaries (e.g. grain boundary dislocations) and twins (e.g. twin fronts viewed as disclination dipoles) may be considered in the framework of multi-defect kinetics [3] as briefly discussed in Section 4. Among other things, this approach may derive results for the interplay between the average nanograin size and the average nanotwin lamellae thickness embedded within. This could possibly lead, in principle, in new ways of designing "super strong" and at the same time "super ductile" nanostructured metals.

3. PHENOMENOLOGICAL MODEL FOR NANOTWINNED METALS

Similarly to the case of nanograined metals, in the case of nanotwinned metals we propose to start with a Voce-type relation used for conventional metals and then modify it by incorporating, in the expression of the relevant flow stress-like quantities, the twin-boundary spacing (or lamella thickness) λ, instead of the grain size d. It should be emphasized that our purpose here is not to present an exhaustive analysis by using the minimal number of phenomenological coefficients and physically justifying the numerical value of every single parameter used. Our purpose is, instead, to show that conventional metal physics modeling may be extended to nanoscopic configurations by properly bringing into the phenomenological description the main and characteristic nanostructural parameters, in a robust and effective manner.

Our starting point will be again a Voce-type stress-strain relation (equivalent to those listed in Eqs. (1) and (4) of the form

$$\sigma = \sigma_s - \left(\sigma_s - \sigma_y\right)\exp\left(-\frac{\left(\varepsilon^p - \varepsilon_y\right)}{\varepsilon_r^p}\right), \qquad (6)$$

where σ_s is the saturation stress, σ_y is the initial yield stress corresponding to the plastic strain ε_y, ε_r^p is the relaxation strain, determining the rate of stress transition from the initial yield stress to the saturation stress. If the value of ε_y is 0.002, then σ_y

is the 0.2% offset yield stress. It should be noted that Eq. (6) is the original one used by Voce and, as already mentioned, it is equivalent to the modified version of Voce relationship given in Eq. (1) or Eq. (4). The form of Eq. (6) is used here, due to the physical interpretation and related microscopic expression given below for the parameter ε_r^p.

As established on both experimental grounds and subsequent physical reasoning, a decrease of the twin thickness leads firstly to a remarkable increase of strength, followed by a substantial decrease of it below a critical twin thickness. Underlying such phenomenon is a transition of the deformation mechanism from HP-type hardening (resulting, in particular, from dislocation pile ups and dislocation transferring across the twin boundaries) to dislocation nucleation controlled IHP-type softening (resulting, in particular, from the nucleation of dislocations at the intersection of a grain boundary with a twin plane and their subsequent movement on the twin plane). The twin thickness-dependent hardening behavior can be described by the conventional HP relationship, with the average grain size parameter (d) replaced by the average twin thickness parameter (λ), as discussed above. Thus, the initial yield stress σ_y and saturation stress σ_s in the Voce model for nt-Cu, when the average twin thickness is larger than a critical value ($\lambda>\lambda_c$), can be written as

$$\sigma_y = \sigma_{y0} + k_1\lambda^{-1/2};\ \ \sigma_s = \sigma_{s0} + k_2\lambda^{-1/2}. \qquad (7)$$

with the index "0" denoting reference value and (k_1,k_2) being phenomenological HP-type strengthening-like parameters. It is noted that an inverse HP component contribution is not included in Eq. (7) as in Eq. (5). This is the case because we will consider the hardening ($\lambda>\lambda_c$) and softening ($\lambda<\lambda_c$) regimes separately here; i.e. we will introduce two different sets of σ-ε constitutive equations reflecting the two different plasticity mechanisms that take place in these regimes, along with different values for the various constitutive parameters used. When the average twin thickness is smaller than λ_c, there are few dislocations in the twin laminas, with most of the dislocation activity taking place on the twin plane where dislocations nucleate from grain boundary-twin intersections and move on the twin plane. As already mentioned, such dislocation source controlled behavior has been revealed in molecular dynamics simulations and a physical strength softening theory was suggested [10] which, in our formulation and terminology, results directly to the following expression for σ_y and σ_s in the IHP type softening regime

$$\sigma_y = \sigma_{y1} - k_3 \ln\left(\frac{d}{\lambda}\right),\ \ \sigma_s = \sigma_{s1} - k_4 \ln\left(\frac{d}{\lambda}\right), \qquad (8)$$

with the index "1" denoting reference value and (k_3,k_4) being phenomenological IHP-type softening-like parameters, whereas d is as usual the average grain size (~500 nm in [11]).

According to Kocks-Mecking model [12], the relaxation strain parameter (ε_r^p) is related to the dynamical process where dislocations annihilate with each other. TEM observations have shown that most of dislocations in nt-Cu accumulated in regions with thickness δ of 7-10 lattice spacings along the twin boundaries [13], while few dislocations exist in the twin laminas. The interaction between mobile and immobile dislocations on the same slip plane, which is the twin plane in nt-Cu, determines the annihilation rate which, in turn, depends on the meeting frequency of the two annihilated dislocations. A non-thermal expression [14] for such process is given by the equation $d\rho/d\varepsilon = C\rho_{TB}$, with C being a constant and ρ_{TB} denoting the local dislocation density in the twin boundary region of thickness δ. Assuming that the critical distance for the annihilation event is 1-10 Burgers vectors, it follows that C should lie in the range of 2-20 [14]. The heterogeneous distribution of the dislocation density in the nt-Cu, gives then the following approximate relationship between ρ_{TB} and the average dislocation density ρ [13], $\rho_{TB} = (\lambda/\delta)\rho$. Combination of the above statements yields

$$\frac{d\rho}{d\varepsilon} = \frac{C\lambda}{\delta}\rho. \qquad (9)$$

The characteristic transient or relaxation strain ε_r^p is finally determined, according to the so-established connection between Voce and Kocks-Mecking models, by the simple expression

$$\varepsilon_\gamma^p = k_5 / \lambda. \qquad (10)$$

This is a linear relationship between ε_r^p and $1/\lambda$ with the value of the coefficient $k_5 = 2\delta/C$ ranging between 0.7-10 Burgers vectors, or 0.17~2.56 nm (the Burgers vector of copper is 0.256 nm).

If we use the Voce-type size-dependent model given by Eq. (6) to fit every stress-strain curve of the ~500 nm nanograined copper with nanoscale twins of varying average thickness one by one, then we can produce a perfect fit of the experimental data by using different sets of parameter values (σ_y,σ_s, ε_r^p) for each one of the six graphs shown. This was, in fact, done in [11] by using the Hollomon-Ludwig relationship ($\sigma = k\varepsilon^n$) and properly adjusting the (k,

n) parameters for each one of the experimental graphs without any further effort on their possible analytical dependence on λ. It can further be seen by adopting the aforementioned procedure that both the the initial yield stress σ_y and saturation stress σ_s follow Eqs. (7) and (8), while the transient strain ε_r^p follows Eq. (10). It is not so important to show these particular fits here (i.e. the individual dependence of σ_y, σ_s, and ε_r^p on λ) since a unified fit for the overall σ-ε (HP/IHP-type) behavior and its dependence on twin thickness will be shown below. It should be pointed out, however, that the curve designated by nt-15 (i.e. nt-Cu with average twin thickness 15 nm) defines the transition between the hard and soft regimes, and that it is fitted by both the HP relation according to Eq. (7) and the IHP relation according to Eq. (8). The gradient plasticity model with interfacial energy used in [15] for determining the critical grain size between hardening and softening regimes in a nanopolycrytral may also serve here as a means to potentially determine the critical thickness where the hardening-softening transition occurs. An alternative method for determining the nanotwin critical thickness (of ~13 nm) was also provided in [16].

In view of the above discussion and the observed/fitting behavior of the parameters (σ_y, σ_s, ε_r^p), a twin thickness-dependent Voce-type expression is obtained through the combination of Eqs. (6), (7), and (10) for the strength hardening regime, i.e.

$$\sigma = \left(\sigma_{s0} + k_2\lambda^{-1/2}\right) - \left[\sigma_{s0} - \sigma_{y0} + \left(k_2 - k_1\right)\lambda^{-1/2}\right]\times \exp\left(-\frac{\left(\varepsilon^p - \varepsilon_y\right)}{k_5}\lambda\right).....\text{hardening}, \quad (11)$$

while a combination of Eqs. (6), (8), and (10) results to the following size-dependent Voce-type expression for the softening regime,

$$\sigma = \left(\sigma_{s1} - k_4 \ln\left(\frac{d}{\lambda}\right)\right) - \left[\sigma_{s1} - \sigma_{y1} - \left(k_4 - k_3\right)\ln\left(\frac{d}{\lambda}\right)\right]\times \exp\left(-\frac{\left(\varepsilon^p - \varepsilon_y\right)}{k_5}\lambda\right).....\text{softening}, \quad (12)$$

The values of the *k* parameters entering in Eqs. (11) and (12) have thus a straight forward physical meaning and correspond to distinct hardening/softening mechanisms which characterize the overall stress-strain behavior of the 500 nm nanograin copper specimens with varying nanotwin thickness. By choosing the values of these hardening/softening coefficients as shown in Table 2, the comparison between model and experiment is shown in Fig. 4a.

In order to improve the fitting, the twin thickness is adjusted by assuming it to be slightly different than the experimentally reported value for the mean thickness [11]. The modified twin thicknesses used for each fitted true stress-strain curve of Fig. 4b are listed in Table 3.

4. NANODEFECT KINETICS

In this final section we list evolution equations for the structural defect populations that emerge at the nanoscale. Such an approach may provide a deeper physical basis for considering strengthening or softening of “nanograin” and “nanotwins” materials. In the case of nanograin materials, the new dominant structural defect populations that need to be con-

Table 2. Parameter values used for the twin thickness-dependent initial yield stress, saturation stress, and transient strain.

	σ_{y0} MPa	k_1 kPa m$^{1/2}$	σ_{s0} MPa	k_2 kPa m$^{1/2}$	σ_{y1} MPa	k_3 MPa	σ_{s1} MPa	k_4 MPa	k_5 nm
Fitted	158	2910	210	3271	2337	422	1847	228	0.562
error	29	176	20	122	354	86	137	33	0.032

Table 3. Modified twin thickness.

λ (nm)	4	8	10	15	35	96
fitted (nm)	4.22	6.94	9.91	17.77	35.24	89.97
error (nm)	0.01	0.02	0.04	0.05	0.23	1.28

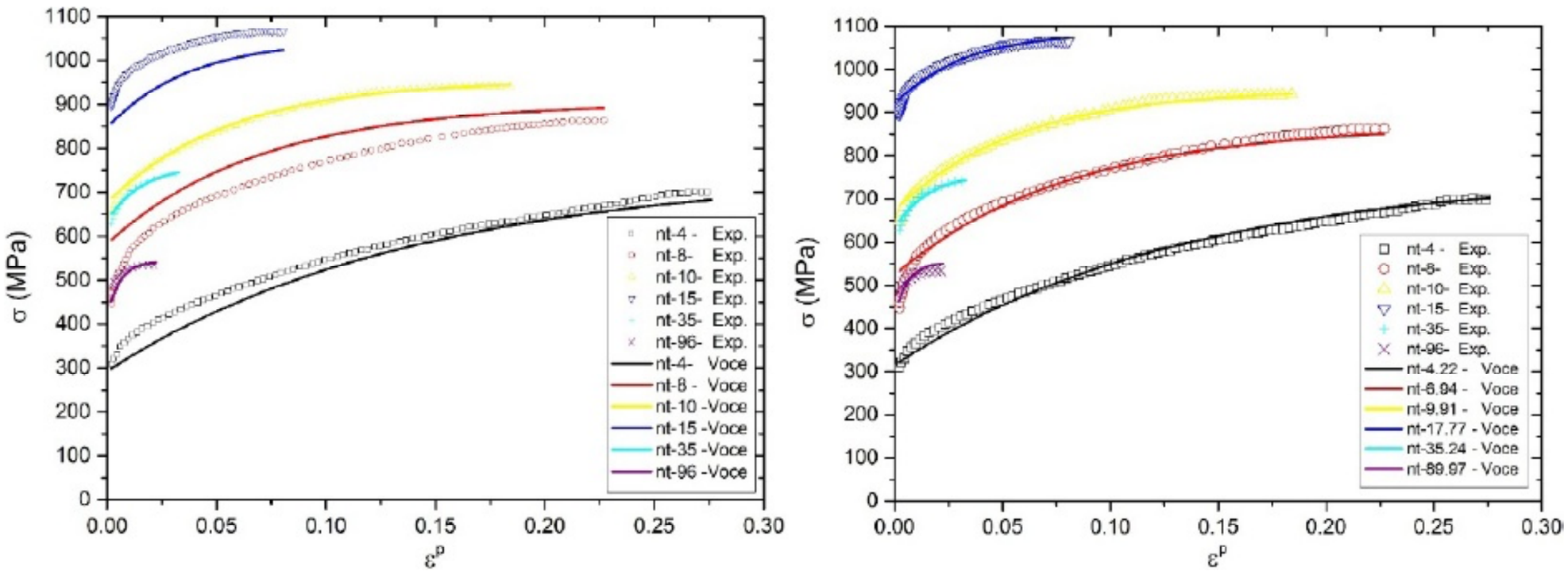

Fig. 4. The fit of the various size-dependent true stress-strain curves for nt-Cu specimens with varying twin thickness. The modified size-dependent Voce model employed was based on Eqs. (11) and (12) with the unique set of the parameter values used for all curves given in Table 2: (a) twin thickness is the same as that reported in [12]. (b) slightly modified twin thickness.

sidered in addition to mobile dislocations and immobile dipoles in the grain interior, are grain boundary sliding dislocations and junction disclinations in triple grain boundary junctions. In the case of nanotwinning, the new dominant structural defect populations to be considered in addition to mobile dislocations are disclination dipoles (twin fronts), twin lamellae, and sessile Lomer-Cottrell dislocations.

4.1. Nanodefect kinetics in nanograined metals

The following populations of defects are distinguished and are characterized by their densities: [17]

ρ - mobile dislocations: they are nucleated and move in the grain interior;

φ - low mobility dislocations: they may be in the form of (nearly immobile) dislocation dipoles evolving in the grain interior;

ψ - grain boundary sliding (mobile) dislocations: they have their Burgers vector parallel to the grain boundary plane;

θ - junction disclinations: they originate from grain boundary dislocations with their Burgers vector normal to the grain boundary plane. Each grain boundary facet may have only two disclinations at its ends. The strength of disclinations relates to the change of the average misorientation at grain boundaries and is designated by ω.

No distinction is made between defects of opposite sign and existing peculiarities of crystallography are neglected. Then, on the basis of appropriate physical considerations concerning the various possible defect mechanisms taking place during deformation, the following system of reaction-diffusion equations may be proposed for the aforementioned defect densities (ρ, φ, ψ, θ):

$$
\begin{aligned}
\frac{\partial \rho}{\partial t} &= A_\rho \rho - B_\rho \rho^2 - C_0 \frac{\rho}{d} + C_3 \rho\varphi + \omega M\theta + N\frac{\Psi}{d} + D_\rho \nabla^2 \rho, \\
\frac{\partial \varphi}{\partial t} &= A_\varphi \rho + B_\varphi \rho^2 - C_4 \rho\varphi - K\varphi + D_\varphi \nabla^2 \varphi, \\
\frac{\partial \Psi}{\partial t} &= C_1 \frac{\rho}{d} + A_\Psi \psi - B_\Psi \psi^2 + D_\psi \nabla^2 \psi, \\
\frac{\partial \theta}{\partial t} &= C_2 \frac{\rho}{\omega d^2} - P_1 \rho\theta - P_2 \psi\theta - G\theta + D_\theta \nabla^2 \theta.
\end{aligned}
\tag{13}
$$

The various physical processes modeled by the terms in the r.h.s. of the above equations may be viewed as “generalized chemical reactions” between different families of defects. These reactions include multiplication of dislocations described by the first term of $(13)_1$. Multiplication of mobile dislocations also contributes directly to the production of immobile dislocations through the first term of $(13)_2$. Grain boundary dislocations also can multiply in a similar way through the second term of $(13)_3$. Mobile dislocations can annihilate through the second term of $(13)_1$ and their “annihilation” gives rise to production of immobile dipoles through the second term of $(13)_2$. Grain boundary sliding dislocations can also annihilate through the third term of $(13)_3$. Mobile dislocations are trapped by grain boundaries through the first term of $(13)_1$. It is important to note that in this

case a size effect is included directly through the dependence of 1/d. These trapped dislocations transform into grain boundary sliding dislocations through the first term of $(13)_3$, and junction disclinations through the first term of $(13)_4$. Other sources of mobile dislocation include: (i) immobile dipole dislocation through the fourth term of $(13)_1$; (ii) activation of dislocation sources by disclination defects through the fifth term of $(13)_1$; and (iii) activation of dislocation sources by the pileups of grain boundary dislocations through the sixth term of $(13)_1$. There is a corresponding reaction accounting for the diminishing of dislocation dipoles through the third term of $(13)_2$. Dislocation dipoles can also disappear during the point defect assisted decay through the fourth term of $(13)_2$. We also assume that disclinations in the junctions can be screened by both mobile dislocations and grain boundary sliding dislocations through the first and third terms of $(13)_4$ respectively. Finally, junction disclinations can loose their activity by absorption of point defects through the fourth term of $(13)_4$.

The mobility of the above families of defects is modeled through diffusion-like terms, i.e. the last terms of Eq. (13) involving the Laplacians. Such diffusion-like motion may be justified on the basis of assuming conservation equations for the total defect densities; thus, defects of opposite sign move in opposite directions with the total density obeying diffusion equation. Diffusion like terms may also result by considering coupling effects with vacancies and other types of structural defects not explicitly accounted for in Eqs (13) and then "adiabatically eliminating" these internal parameters which are viewed as the fast variables of the system. The "diffusion-like" coefficients (D_ρ,D_φ,D_ψ,D_θ) should be determined by considering the mobility of the individual defects, their geometry and their interaction with the lattice; and in first approximation one may set $D_\varphi > D_\theta \geq 0$. Various simplified versions of Eqs. (13) may thus be adopted and stationary solutions may be derived along with their stability properties as a function of the grain size.

4.2. Nanodefect kinetics in nanotwinned metals

Alternative nanodefect populations and nanodefect kinetics emerge in the case of nanotwinning. In this case, four different defect populations may be introduced: ρ – mobile dislocations; θ – disclination dipoles (twin fronts); φ – twin lamellae; ξ – sessile Lomer-Cotrell dislocations. Then, the following evolution equations may be proposed to model coupled dislocation-nanotwinning processes:

$$\begin{aligned}
\frac{\partial \rho}{\partial t} &= A_0\rho - A_1\rho^2 - B_1\rho\xi + F_1\theta\xi - \\
&G_1\theta\xi\rho - K_1\rho\phi + N_1\theta\phi + D_\rho \frac{\partial^2 \rho}{\partial x^2}, \\
\frac{\partial \theta}{\partial t} &= B_2\rho\xi + G_2\theta\rho\phi + K_2\rho\phi - R\theta^2 + D_\theta \frac{\partial^2 \theta}{\partial x^2}, \\
\frac{\partial \phi}{\partial t} &= E_0\theta - K_3\rho\phi - N_2\theta\phi, \\
\frac{\partial \xi}{\partial t} &= A_2\rho^2 - F_2\theta\xi.
\end{aligned} \tag{14}$$

The physical meaning of the various terms in the r.h.s. of Eqs $(14)_1$- $(14)_4$ is as follows: The term $A_0\rho$ describes the activity of dislocation sources. The term with coefficient A_1 describes the disappearance of mobile dislocations due to the formation of Lomer-Cotrell sessile dislocations and partly due to annihilation. There is a corresponding term in Eq. $(14)_4$ which describes the input for Lomer-Cotrell dislocations; however the coefficients A's in Eqs. $(14)_1$ and $(14)_2$ don't need to be equal and, thus, two rate constants A_1 and A_2 are introduced. The term with coefficient B_1 in $(14)_1$ corresponds to dislocation pile-up formation with a follow-up transformation into mobile dipole fronts θ, as indicated by the B_2 term of Eq. $(14)_2$. The F_1 term describes processes of Lomer-Cotrell barriers dissociation in the field of disclination dipoles and the production of mobile dislocations p; the corresponding sink F_2-term manifests itself in Eq. $(14)_4$. A third order nonlinearity appears in the G-terms which designate complex reactions initiated by θ transforming ρ dislocations into mobile twins (G_1) in the vicinity of Lomer-Cotrell dislocations, as well as in the corresponding input for disclination dipoles (G_2). The production of new mobile twin fronts (disclination dipoles) θ is possible due to the reaction between mobile dislocations and twin lamellae – the K_2-term in Eq. $(14)_2$. This reaction contributes simultaneously to Eq. $(14)_1$ (sink term with K_1 for ρ) and to Eq. $(14)_3$ (sink term with K_3 for φ). Mobile twin fronts can destruct twin lamellae resulting to the production of mobile dislocations: the N_1-term is responsible for this process and a related sink term in Eq. $(14)_3$ involves the coefficient N_2. Finally, it is noted that there are also two special reactions which involve the density of one-type of defects only: (i) the R-term in Eq. $(14)_2$ describing disclination dipole annihilation (no other defects appear as a result of this reaction); and (ii) the E_0 source term in Eq. $(14)_{3-}$ describing the production of twin lamellae

due only to the mobility of twin fronts ($E_0 < \nu_\theta$;ν designates the velocity of dislocation dipoles).

Various simplifications can be introduced in Eqs. (14), as in the case of Eqs. (13), and stationary solutions can be derived. In a future publication by the last two authors such considerations for Eqs. (13) and (14) will be explored with emphasis on stability analysis. This analysis, along with appropriate expressions for the stress/strain macroscopic variables in terms of the defect populations (dislocations, disclinations, twins) may result to size-dependent flow curves and stability assessments for the overall mechanical behavior at the nanoscale.

5. CONCLUSIONS

A composite model for nanograin and nanotwin materials is adopted leading to Voce type constitutive equations containing the grain size (d) or the twin lamella thickness (λ) in the plasticity parameters entering the aforementioned modified Voce model. Experimentally obtained size-dependent flow curves for nanocrystalline (nc) and nanotwin (nt) metals can be conveniently interpreted by the proposed unified phenomenological model. These curves exhibit a Hall-Petch (HP) type of behavior, i.e. material strengthening, as the grain size or twin thickness is reduced down to a critical value. Further reduction of d or λ results to an inverse Hall-Petch (IHP) type of behavior, i.e. material softening. Finally, a nanodefect kinetics approach is suggested for nc and nt metals by focusing on the new defect populations (grain boundary dislocations, disclinations, twins) that emerge when the nanoscopic deformation processes and their couplings need to be considered.

ACKNOWLEDGEMENTS

XZ is grateful for the support of National Natural Science Foundation of China (11202172), China Postdoctoral Science Foundation (2013M530405), the Basic Application Research Plan of Sichuan Province (2015JY0239) and the Sichuan Provincial Youth Science and Technology Innovation Team (2013TD0004). The authors also acknowledge the support of Aristotle University through the Aristeia-II and Hellenic ERC-13 grants of the General Secretariat for Research and Technology (GSRT) of Greece.

REFERENCES

[1] E. Voce // *Metallurgia* **51** (1955) 219.
[2] K.E. Aifantis and A.A. Konstantinidis // *Mater. Sci. Eng. A* **503** (2009) 198.
[3] X. Zhang, A.E. Romanov and E.C. Aifantis, In: *Proc. 5th International Conference on Nanomaterials by Severe Plastic Deformation, NanoSPD5* (2011), p. 991.
[4] X. Zhang, K.E. Aifantis, J. Senger, D. Weygand and M. Zaiser // *J. Mater. Res.* **29** (2014) 2116.
[5] K.E. Aifantis and J.R. Willis // *J. Mech. Phys. Solids* **53** (2005) 1047.
[6] K.E. Aifantis, W.A. Soer, J.T.M. De Hosson and J.R. Willis // *Acta Mater.* **54** (2006) 5077.
[7] B. Farrokh and A.S. Khan // *Int. J. Plast.* **25** (2009) 715.
[8] J. Schiøtz, T. Vegge, F.D. Di Tolla and K.W. Jacobsen // *Phys. Rev. B* **60** (1999) 11971.
[9] R. Schwaiger, B. Moser, M. Dao, N. Chollacoop and S. Suresh // *Acta Mater.* **51** (2003) 5159.
[10] X. Li, Y. Wei, L. Lu, K. Lu and H. Gao // *Nature* **464** (2010) 877.
[11] L. Lu, X. Chen, X. Huang and K. Lu // *Science* **323** (2009) 607.
[12] Y. Estrin and H. Mecking // *Acta Metall*. **32** (1984) 57.
[13] L. Lu, Z.S. You and K. Lu // *Scripta Mater*. **66** (2012) 837.
[14] A. Ma and F. Roters // *Acta Mater.* **52** (2004) 3603.
[15] X. Zhang and K.E. Aifantis // *J. Mater. Res*. **26** (2011) 1399.
[16] L. Zhu, H. Ruan, X. Li, M. Dao, H. Gao and J. Lu // *Acta Mater*. **59** (2011) 5544.
[17] E.C. Aifantis // *IOP Conference Series: Materials Science and Engineering* **63** (2014) 012129.